ADVANCED ENERGY MATERIALS

Supporting Information

for *Adv. Energy Mater.,* DOI: 10.1002/aenm.202101594

High Depth-of-Discharge Zinc Rechargeability Enabled by a Self-Assembled Polymeric Coating

*David J. Arnot, Matthew B. Lim, Nelson S. Bell, Noah B. Schorr, Ryan C. Hill, Andrew Meyer, Yang-Tse Cheng, and Timothy N. Lambert**

Supporting Information

High Depth-of-Discharge Zinc Rechargeability Enabled by a Self-Assembled Polymeric Coating

David J. Arnot,[a‡] Matthew B. Lim,[a‡] Nelson S. Bell,[b] Noah B. Schorr,[a] Ryan Hill,[c] Andrew Meyer,[c] Yang-Tse Cheng[c] and Timothy N. Lambert[a]*

[a]Department of Photovoltaics and Materials, Sandia National Laboratories, Albuquerque, NM, 87185-0734, USA
[b]Advanced Materials Laboratory, Sandia National Laboratories, Albuquerque, NM, 87185-0734, USA
[c]Department of Chemical and Materials Engineering, University of Kentucky, KY, 40506, USA
[‡]These authors contributed equally to this work.
[*]E-mail: tnlambe@sandia.gov

1. Additional Experimental Details

1.1. Materials

Battery-grade alloyed Zn powder (BIA 60 200 65 d175) was obtained from EverZinc. Zinc oxide (ZnO; 99.00%, certified ACS) and tartaric acid (> 99.0%) were purchased from Fisher Scientific. Sodium dodecylbenzenesulfonate (SDBS; technical grade, 88%) was purchased from Acros Organics. Polytetrafluoroethylene (PTFE; DISP 30, ~60 wt.% aqueous dispersion) was obtained from Chemours. Potassium hydroxide (KOH; 90%, flakes) and polyethylene glycol 400 (PEG 400) were purchased from Sigma-Aldrich. Nafion D-521 dispersion (5% w/w in water and 1-propanol) was obtained from Alfa Aesar. Expanded Cu mesh (5CU6-060DBFA) was purchased from Dexmet Corporation. Nickel welding strips (spooled, 6 mm width x 0.1 mm thickness) were obtained from MTI Corporation. Celgard 3501 separators were obtained from Celgard LLC, and cellophane 350P00 separators from Innovia Films Inc. Cellulose fiber tissue was purchased from Kimberly-Clark. Acrylonitrile butadiene styrene (ABS) shims (1-3/8” wide, ¼” thick) were purchased from McMaster-Carr. Polypropylene battery cases (Flex-

A-Top, FT9, 1 ½" W x 5/8" D x 2 ½" H) were purchased from LA Container Inc. Double sided tape (410M) was purchased from 3M Company. Sintered NiOOH electrode sheets (~0.65 mm thick including current collector) were purchased from Jiangsu Highstar Battery Manufacturing. All materials and reagents were used as received, without further purification.

1.2. Contact Angle and Self Assembly

Contact angle measurements using probe fluids with van Oss theory are used to determine the surface properties of the coated separator membranes. The adsorption of Nafion from solution to a substrate relates to the state of dispersion of the ionomer in solution, and attractive interactions of the Nafion to the surface. Ionomer structure in solution is largely dependent upon the solvent composition through wetting and solvent parameters.[1-2] Paul et al.[3] varied film thickness by varying solution stability and aggregation dependent upon solvent composition. They found that film thickness affects surface properties, as layers of 55 nm or less remained hydrophilic rather than the expected hydrophobic behavior of the fluoropolymer. Very thin films can counterintuitively have very high surface polarity as a result. Wang et al.[4] imaged the structure of films cast from a variety of solvents, finding these films vary in their microstructure by the size and distribution of the ionic domain size in each film. Film structure is dependent on the water content of the film. Polar ionic domains phase-segregate and are treated as bundles of aligned inverted micelles having a "macaroni" shape (ionic domains create water filled microphase within a hydrophobic shell) for dehydrated films where the continuous phase is based on the fluoropolymer. If hydration increases, the structure is expected to invert, where the micelles express their ionic domains as a "spaghetti" structure, where the continuous phase is the fluid phase.[5] This has been noted in the contact angle behavior of Nafion films, as normally the surface of Nafion is quite hydrophobic, with a contact angle > 105°. However, the surface can switch to expose sulfonate character when in contact with water, with a change in

surface roughness. This leads to a high contact angle hysteresis post wetting, and a low receding contact angle.[5-6]

The attraction of Nafion to a surface relates to the ionic attraction of the surface groups, or wetting interactions of the fluoropolymer to the solid interface. Cationic surfactants would exhibit an electrostatic attraction to the sulfonate groups. Nafion films are known to form interphases with nonpolar surfactants in solution such as Pluronics and polyethylene oxide.[6-7] Nafion is expected to associate with polyethylene or polypropylene through the similarity of the backbone chains as $-CH_2-CH_2-$ and $-CF_2-CF_2-$. Residual water is expected to be segregated to the ionic domain as an interphase.

Nafion-Celgard composite coatings were formed by the solution exposure and adsorption method as described in the Experimental section of the main text. In addition, thick Nafion coatings were drop cast from solution, to contrast with the solution adsorption method. Approximately 2 mL of Nafion dispersion was placed over the Celgard 3501 and allowed to dry overnight in ambient laboratory conditions. The commercial-off-the-shelf (COTS), drop cast Nafion, and NC-Celgard separators were mounted in a 3D-printed circular frame that stretched each membrane taut over an air gap to form a suspended flat surface for imaging of contact angle. The contact angle of each separator was measured using deionized water (18 MΩ-cm, Millipore), diiodomethane (Sigma Aldrich, 99.9%), and ethylene glycol (Sigma Aldrich, 99.9%) as the probe liquids. These liquids were used as received without further purification in air. The contact angle was measured over the supported films, and error was increased to ~5 degrees from the buckling or deformation of the fluid drops. The contact angle for each separator was measured with a VCA Optima model S/N unit (AST Products, Inc.), using a minimum of five drops and recording the contact angle on the left and right side of each drop.

The properties of the surfaces were measured using the van Oss theory, with established interaction energy parameters based on the Lifshitz van der Waals (LW), Lewis electron

acceptor (+) and Lewis electron donor (-) properties. The surface energy parameters are derived from the complete Young-Dupré equation (Equation S1) to determine the factors for the solid surface as the London-van der Waals γ_s^{LW}, electron accepting γ_s^+, and electron donating γ_s^- characteristics of the surfaces.[8]

$$\frac{(1+cos\,\theta)\gamma_L}{2} = \left(\sqrt{\gamma_s^{LW}\gamma_L^{LW}} + \sqrt{\gamma_s^+\gamma_L^-} + \sqrt{\gamma_s^-\gamma_L^+}\right) \quad \text{(S1)}$$

The contact angle values are presented in Table S1. Table S2 provides reference values for the van Oss parameters.

Each surface measured can be solved for the three surface properties using Equation S1 and the contact angle for each fluid. With these parameters, the surface energy of the solid can be calculated from the contact angles and the fluid surface tension parameters using equation S2. The determined values are provided in Table S3.

$$\gamma_S = \gamma_s^{LW} + 2\sqrt{\gamma_s^+\gamma_s^-} \quad \text{(S2)}$$

The measured surface energy parameters for COTS Celgard 3501 and cellophane 350P00 are close to the published values for polypropylene and cellulose respectively from van Oss,[8] included in Table S2. The measured Lifshitz-van der Waals (dispersive) term for cellophane is lower than the published value for cellulose, and the (-) value is higher than expected, but the trends are similar to that from literature. Likewise, the Celgard was compared to polypropylene, which in literature is nonpolar and has very low values for the polar (-) and (+) surface energy components. The values we determined were higher than literature, which could be due to the surfactant coating on Celgard 3501.[9] Nevertheless, the polar components remain very small, and the LW term at 28.7 is in reasonable agreement with that of the published value of 25.

The surface properties of both the solution processed and thick dried Nafion coatings are similar, and of comparable properties to prior literature publications. The surface energy

terms for NC-Celgard are similar to those reported by Paul et al.[3] for a 160-nm self-assembled Nafion film on a SiO_2/Si wafer, which differ somewhat from bulk Nafion (Table S2). Interestingly, the LW terms for NC-Celgard and the 160-nm Nafion film are lower than that reported by van Oss for Teflon FEP (17.9 mJ m^{-2}), which is expected to be the lower limit for materials due to the low dielectric constant. We note, however, that this may be an artifact of variability in measurement conditions, as literature values for γ_s^{LW} of Teflon vary between 14.6 and 25.8.[3] Nafion films are expected to behave similarly to Teflon with respect to the dispersive component of the interaction energy, due to the polytetrafluoroethylene backbone of Nafion. However, Nafion should have a higher polar component, with basic character, due to the sulfonate side groups on the polytetrafluoroethylene backbone.[10] This is supported by the measured γ_s^- of 4 mJ m^{-2} compared to the γ_s^+ of 1.4 mJ m^{-2} for Nafion. In the NC-Celgard, the polar term γ_s^- is even higher at 7.2 mJ m^{-2}. This suggests that the films formed have higher exposure of ionic domains than bulk Nafion films tested in the literature.

1.3. Battery Assembly

Current collectors for the Zn anode were prepared by cutting Cu mesh to the same size as the anode (¾ x 1 inch) and spot-welding a Ni tab to the left edge of the mesh. Cathodes were prepared by cutting out rectangles from the as-received sheet of sintered NiOOH, with a coated area of ¾ x 1 inch (for 20-DOD cells) or 1 x 1 inch (for 50-DOD cells) and an additional ¼ inch-wide strip of bare Ni current collector on the left side, to which a Ni tab was spot-welded. After wrapping, the electrodes were placed in a cell case with one ABS shim and 4 mL electrolyte (for 20-DOD cells) or 3 mL electrolyte (for 50-DOD cells). After soaking overnight, a second ABS shim was inserted to fully compress the electrode assembly, and 1 mL electrolyte (for 20-DOD cells, for a total electrolyte volume of 5 mL) or 1.3 mL electrolyte (for 50-DOD, for a total electrolyte volume of 4.3 mL) was added.

1.4. Peel Testing

Based on the ASTM D903 standard, 180° peel tests were carried out using an IMADA force measurement station with a 5 N load cell. Separator samples of 1 x 8 cm were prepared. The setup for the test is shown in Figure S5a. In short, an NC-Celgard separator was placed between two pieces of double-sided tape (410M, 3M Company). The bottom piece of tape was attached to a stationary stainless-steel plate. The top piece of tape was then pulled at a rate of 60 mm min^{-1} to delaminate the Nafion coating. Since the separator was coated on both sides, the sample could delaminate at either the top or bottom interface. During peeling, a plateau in the load vs. time curve would occur, indicating the steady peeling of the coating. The load during this plateau was averaged and divided by the sample width to calculate the peel strength. To better understand the mechanical strength of the Nafion coating and the effect of placing the separator in alkaline electrolyte, peel tests were performed on as prepared NC-Celgard, NC-Celgard soaked in solutions of 32 wt.% KOH for 72 h, and NC-Celgard soaked in solutions of ZnO-saturated 32 wt.% KOH for 72 h. After soaking in electrolyte, the separators were washed with deionized water and dried in ambient air. Note that the values obtained here should be primarily used for comparative purposes between each other and more rigorous analysis would be required for reliable quantitative results.

2. Supporting Figures and Tables

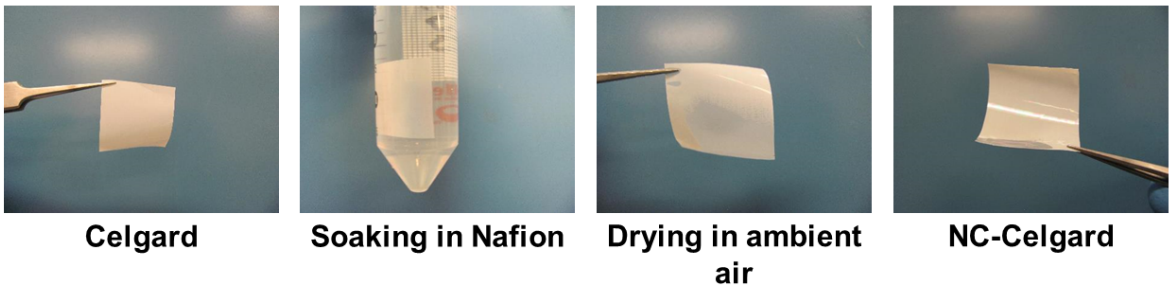

Figure S1. Images showing the simple dip-coating process used to make the NC-Celgard separators.

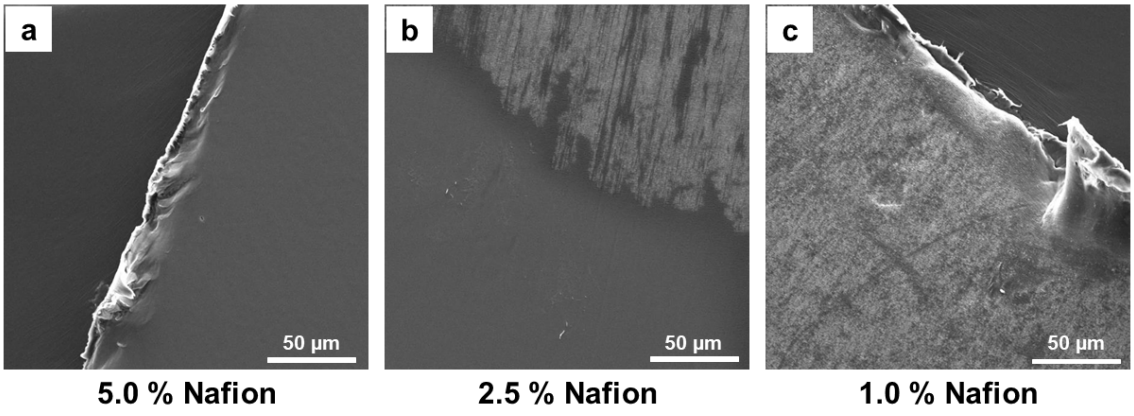

Figure S2. Celgard immersed for 20 h in Nafion solutions of **a)** 5.0%, **b)** 2.5%, and **c)** 1.0% concentrations. Concentrations lower than 5.0 % give inconsistent coverage.

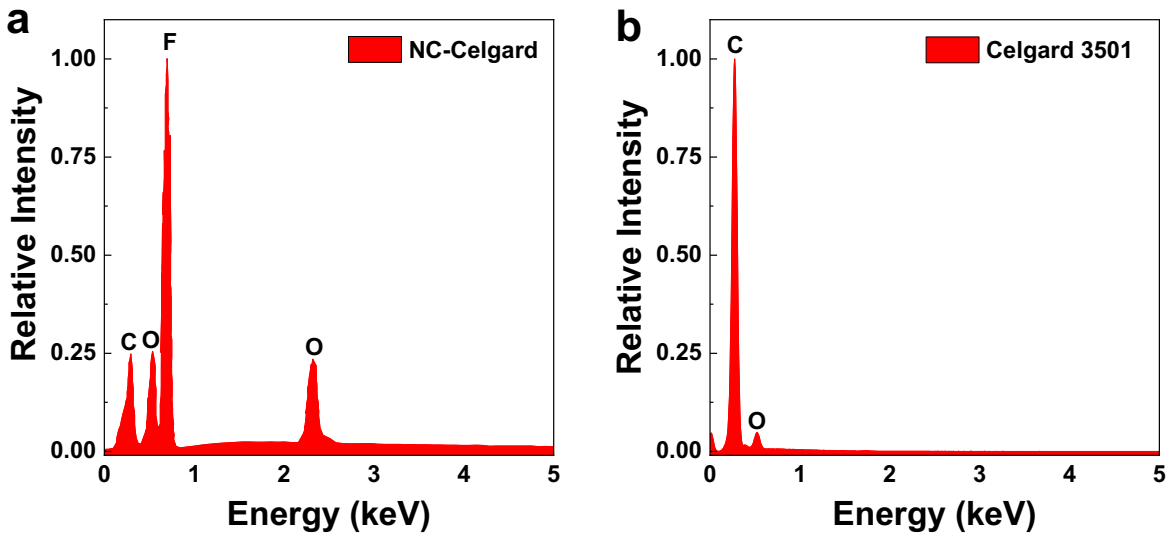

Figure S3. EDS spectrum of **a)** NC-Celgard confirms the Nafion coating with a strong fluorine signal at 0.69 keV. **b)** The unmodified Celgard separator showed a strong carbon signal as well as a peak at 0.53 keV associated with oxygen, likely a component of the surfactant used to improve separator wetting. Weak nitrogen and silicon peaks were also present in the Celgard spectrum.

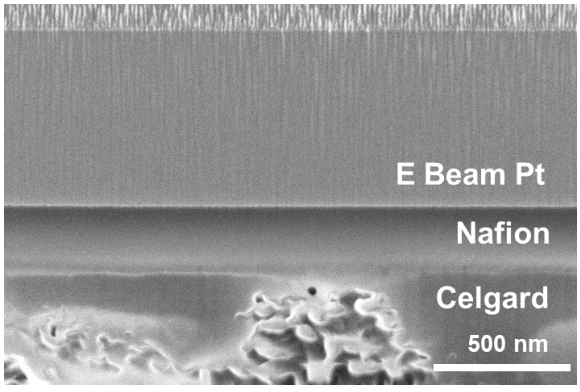

Figure S4. Cross-sectional SEM image of Celgard immersed in a 5% Nafion solution for one week. The longer soak time produced a coating thickness of about 270 nm.

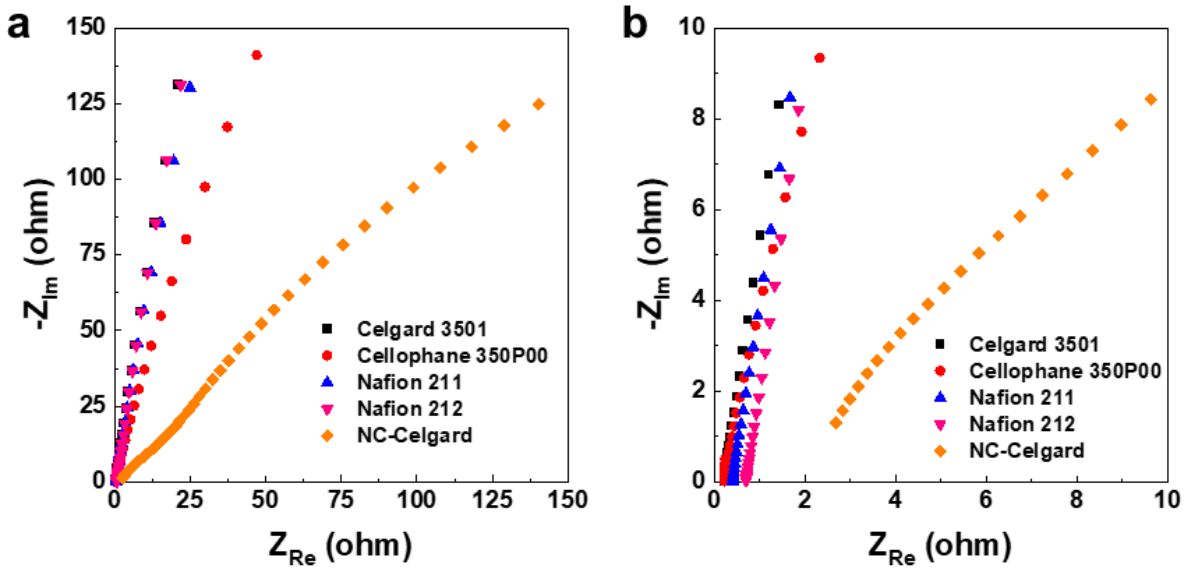

Figure S5. a) Nyquist plot of the NC-Celgard and commercial separators. The intercept with the real axis was used as the bulk resistance of the separator in conductivity calculations. In the case of NC-Celgard, a linear extrapolation from the last 5 points was used to find the intercept. **b)** The same plot with a smaller axis scale.

Table S1: Contact Angles of Probe Liquids on Commercial and NC-Celgard Separators

Substrate	Liquid	Average Contact Angle (degrees)	Standard Deviation
Celgard 3501	Water	102.9	2.8
	Ethylene Glycol	74.9	5.7
	Diiodomethane	59.8	3.2
Cellophane 350P00	Water	38.5	3.2
	Ethylene Glycol	11	1.9
	Diiodomethane	40.1	3.9
Nafion (drop cast)	Water	112.5	5.5
	Ethylene Glycol	102.8	5.8
	Diiodomethane	82.6	3.2
NC-Celgard	Water	112.7	1.5
	Ethylene Glycol	109.4	4.7
	Diiodomethane	87.4	1.9

Table S2: Tabulated Values of Surface Energy Parameters from van Oss,[8] Paul et al.,[3] and Kim et al.[10]

Material	γ_s^{LW} [mJ m^{-2}]	γ_s^+ [mJ m^{-2}]	γ_s^- [mJ m^{-2}]	Polar (AB) $(2\sqrt{\gamma_s^+\gamma_s^-})$ [mJ m^{-2}]	γ_S [mJ m^{-2}]
Water[8]	21.8	25.5	25.5	51	72.8
Ethylene Glycol[8]	29	3	30.1	19	48
Diiodomethane[8]	50.8	0	0	0	50.8
Polypropylene[8]	25.7	0	0	0	25.7
Cellulose[8]	44	1.6	17.2	10.5	54.5
Teflon FEP[8]	17.9	0	0	0	17.9
Teflon[3]	14.6–25.8	0–0.8	0–3.0	0–2.7	14.7–26.0
Nafion film (160 nm)[3]	14.1	0.5	5.8	3.4	17.5
Nafion membrane[10]	12.7	0.1	6.0	1.5	14.2

Table S3: Surface Parameters from Contact Angle Probe Fluid Measurements

Substrate	γ_s^{LW} [mJ m^{-2}]	γ_s^+ [mJ m^{-2}]	γ_s^- [mJ m^{-2}]	γ_S [mJ m^{-2}]
Celgard 3501	28.7	0.007	0.31	28.8
Cellophane 350P00	39.5	0.17	43.4	45
Nafion (drop cast)	16.2	1.4	4	21.0
NC-Celgard	13.9	2.5	7.2	22.4

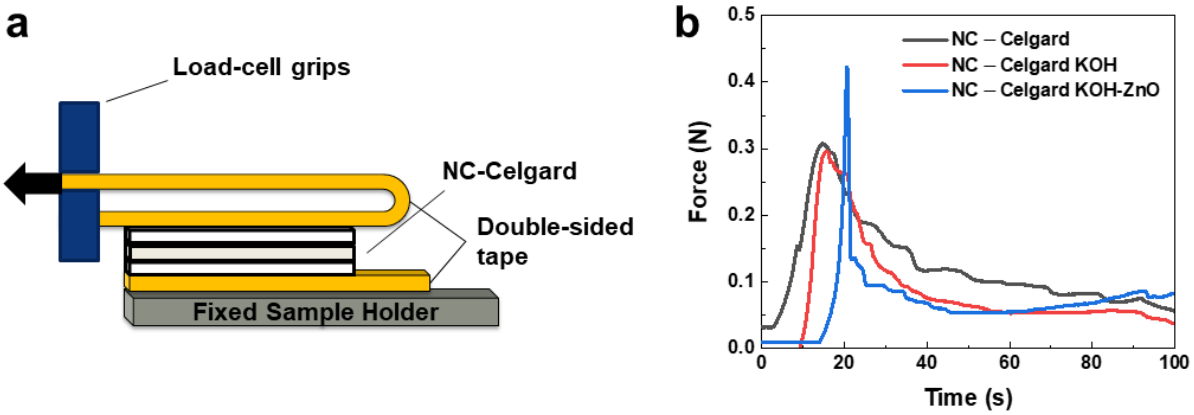

Figure S6. a) The experimental setup used for peel testing. **b)** Typical force versus time curves for the tested separators showing higher peel strength for as prepared NC-Celgard compared to NC-Celgard soaked in KOH and ZnO-saturated KOH solutions. Note that the differing forces at the start of the test are an artifact of setting up the experiment and do not affect the rest of the measurement.

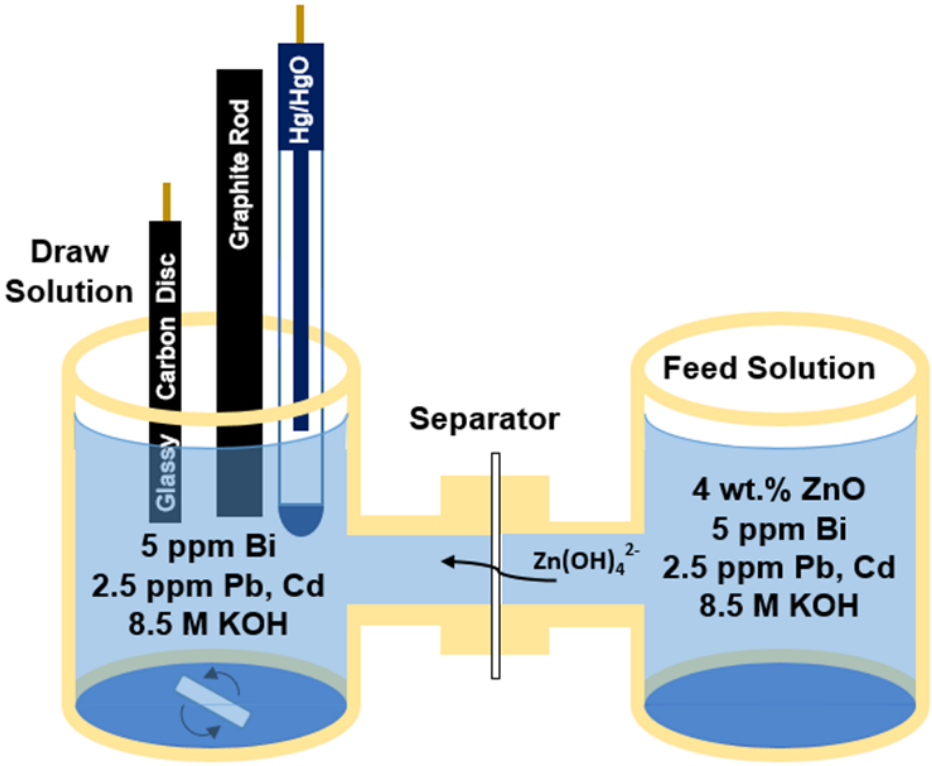

Figure S7. A diagram of the test cell used for Zn and OH- crossover testing. Solution concentrations shown here are for Zn crossover testing.[11]

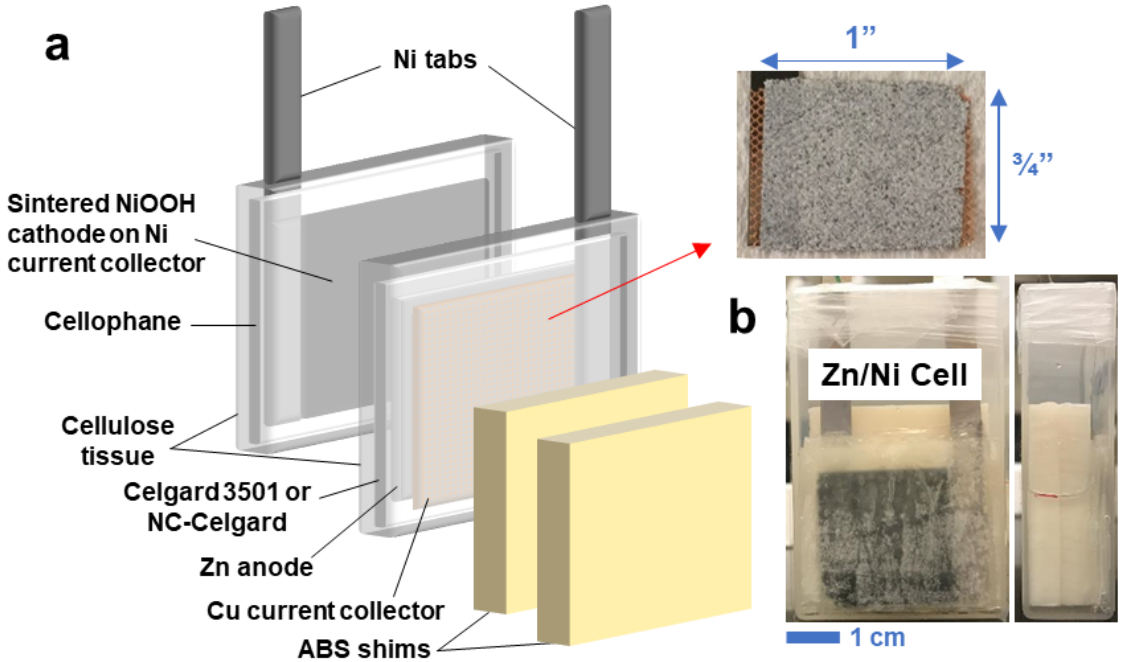

Figure S8. a) Schematic depicting the assembly of our Zn–Ni batteries with a photograph of a pristine anode after pressing onto the Cu current collector (top right). **b)** Photograph of front and side of a fully assembled 50-DOD cell.

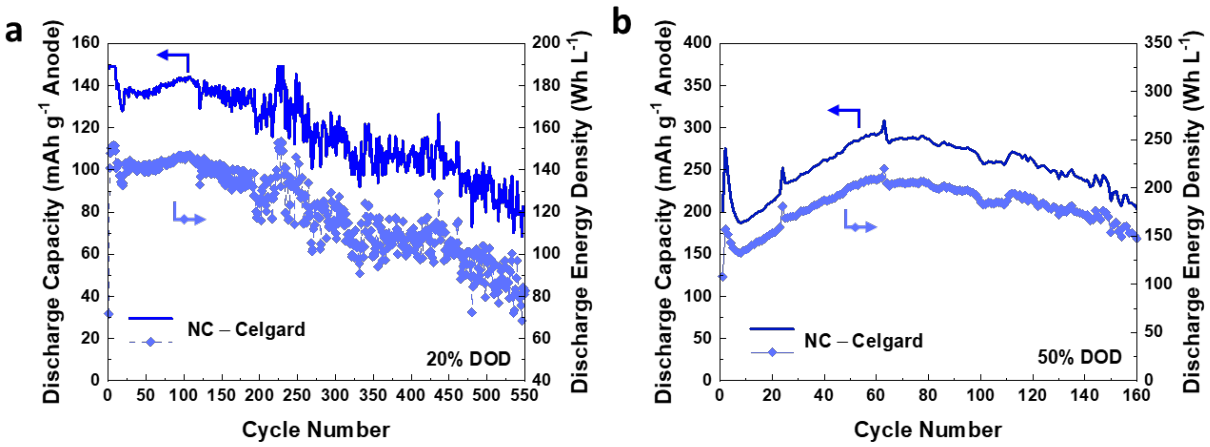

Figure S9. Discharge capacity and energy density, defined relative to volume between and including the current collectors for **a)** 20-DOD-NC cells (0.605 cm^3), and **b)** 50-DOD-NC cells (0.806 cm^3).

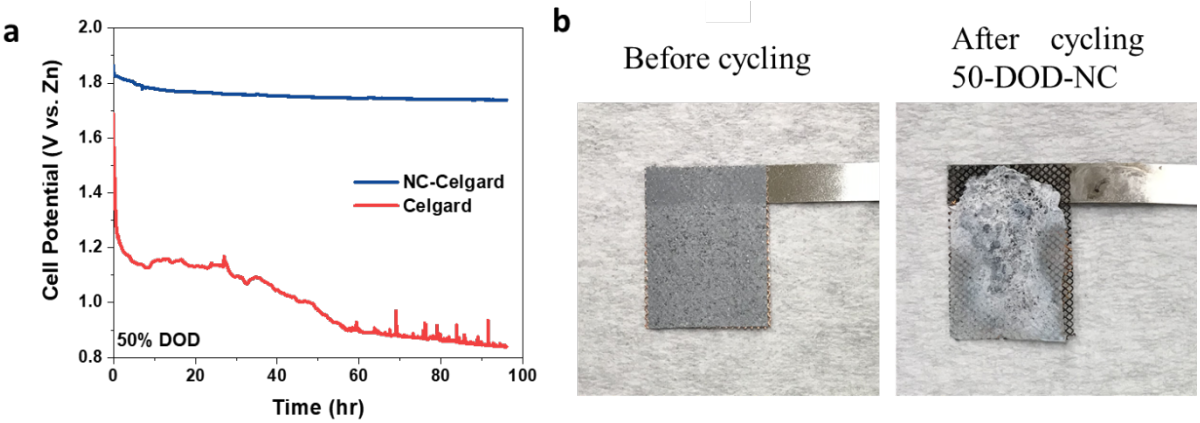

Figure S10 Post cell cycling analysis. **a)** Open-circuit potential of cells over 96 h immediately following the final charge. **b)** Photographs of Zn anode before and after cycling at 50-DOD-NC conditions showing the shape change of the Zn-anode.

3. Comparison of Zn–Ni Cycling Performance to the Literature

To compare the performance and practical relevance of our Zn–Ni cells with Nafion-coated separator to other alkaline zinc battery developments, we adopted the approach of Stock et al. who introduced seven quantitative performance descriptors in a recent review:[12] mass ratio of active material to anode mixture (m_{AM} / m_{anode}), ratio of active material capacity to electrolyte volume (Q_{AM} / V_E) , number of cycles (N_C), averaged coulombic efficiency ($\bar{\Phi}_Q$), averaged utilization of active material ($\bar{X}_{AM}$), averaged discharge capacity per mass of anode mixture ($\bar{q}_{dis}$), and the product of N_C and $\bar{q}_{dis}$. High values of these metrics are more desirable and more commercially practical. While the significance of these metrics is explained at length in the review and may be self-evident, we reiterate several important points here. First, normalizing the discharge capacity to the mass of overall anode mixture (as opposed to the active mass as is often done in the literature) accounts for the presence of inactive additives. Second, Q_{AM} / V_E accounts for unrealistically large excesses of electrolyte, as in a beaker cell, which can significantly impact Zn anode behavior at high utilization.[13] Third, $N_C \cdot \bar{q}_{dis}$ combines retention and utilization into a single metric that allows for simple comparison of cycle life between studies that employ different levels of Zn utilization. Stock's review calculated these seven metrics for 70 references on alkaline Zn anode developments, showing that most of them have high values for only one or two of the metrics.

Table S4 lists these values for our 50-DOD-NC and 20-DOD-NC cells, alongside other recent literature reports showing high reversible zinc utilization in Zn–Ni cells (several of which are included in Stock's review). In addition, we tabulate the areal capacity of each anode (Q_{AM} / A_{anode}), the ratio of capacity in the electrolyte to the capacity of solid active material in the anode (Q_E / Q_{AM}), and the areal applied current density during discharge and charge (j_{dis} and j_{ch} respectively). Q_{AM} / A_{anode} former accounts for the effect of low-density anodes or very thin anodes, which may have a high gravimetric active loading but are still impractical. As an example in the table, Yan et al.[14] reported a lasagna-like anode material of ZnO nanoparticles

encapsulated within graphene oxide sheets, where the mass fraction of active material in the anode was 0.71 but the casted electrode was so thin (5 μm) that the areal loading of ZnO was only ~1 mg cm^{-2} or 0.66 mAh cm^{-2}. Q_E / Q_{AM} accounts for the possible presence of Zn salts within the electrolyte formulation. As we have noted in our previous study of ZnO-saturated electrolytes in Zn–Ni cells,[15] if a system has a large amount of zinc species in the electrolyte relative to the anode, these pre-dissolved species can also participate in redox reactions, artificially inflating the specific capacity and active material utilization of the anode if left unaccounted for. Where applicable, we have noted how much the reported specific capacity and utilization are reduced when accounting for the pre-dissolved Zn species. Finally, the areal current densities allow for easy comparison of rate performance between studies, as opposed to C-rate which depends on the amount of active material in the electrode.

Both our 50-DOD-NC and 20-DOD-NC cells feature high $N_C \cdot \bar{q}_{dis}$ (≥ 40, comparable to the three-dimensional Zn sponge anodes reported by Parker et al.[16]), along with energy-dense anodes (m_{AM} / m_{anode} = 0.929, $Q_{AM} / A_{anode} \approx 60$), and relatively low amounts of electrolyte ($Q_{AM} / V_E > 57$). This shows the promising performance and practicality of our system in addition to our simple self-assembled separator and pasted zinc electrodes, which are already compatible with scalable roll-to-roll processes.

Table S4. Comparison of our Zn–Ni cells with Nafion-coated separator to other recent reports of high zinc utilization in alkaline Zn–Ni systems.

Reference	Anode Composition	Electrolyte	Q_{AM}/A_{anode} [mAh cm^{-2}]	m_{AM}/m_{anode}	Q_{AM}/V_E [mAh mL^{-1}]	Q_E/Q_{AM}	j_{dis}; j_{ch} [mA cm^{-2}]	$\bar{X}_{AM}$ [%]	$\bar{q}_{dis}$ [mAh g^{-1} anode]	$\bar{\Phi}_Q$ [%]	N_C	$N_C \cdot \bar{q}_{dis}$ [Ah g^{-1}]	Notes
This work (50-DOD-NC)	83.1% Zn, 9.8% ZnO, 2.2% SDBS, 4.9% PTFE	32% KOH + 4000 ppm tartaric acid + 3000 ppm PEG400	59.9	0.929	67.4	0	3.0; 3.0	32.4	242	77.3	164	39.7	
This work (20-DOD-NC)	83.1% Zn, 9.8% ZnO, 2.2% SDBS, 4.9% PTFE	32% KOH + 4000 ppm tartaric acid + 3000 ppm PEG400	59.2	0.929	57.3	0	1.5; 1.5	15.9	118	75.6	550	65.1	
Lim et al., 2020[15]	83.1% Zn, 9.8% ZnO, 2.2% SDBS, 4.9% PTFE	32% KOH + 4000 ppm tartaric acid + 3000 ppm PEG400, saturated with ZnO	57.4	0.929	92.7	0.427	5.7; 5.7	31.6	337	93.2	105	35.4	[A]
Lim et al., 2020[15]	83.1% Zn, 9.8% ZnO, 2.2% SDBS, 4.9% PTFE	32% KOH + 4000 ppm tartaric acid + 3000 ppm PEG400, saturated with ZnO	58.5	0.929	94.3	0.420	5.8; 5.8	20.7	219	93.8	174	38.1	[A]
Lim et al., 2020[15]	83.1% Zn, 9.8% ZnO, 2.2% SDBS, 4.9% PTFE	32% KOH + 4000 ppm tartaric acid + 3000 ppm PEG400, saturated with ZnO	57.9	0.929	93.4	0.424	5.8; 5.8	13.9	148	94.2	259	38.3	[A]
Turney et al., 2017[13]	64.5% ZnO, 25% $Ca(OH)_2$, 8% Bi_2O_3, 2.5% PTFE	25% KOH	70-140	0.645	612	0	6.5; 6.5	13.6	57.7	80	1000	57.7	[B]
Parker et al., 2017[16]	89% 3D Zn sponge (with 300 ppm In + 300 ppm Bi), 11% $Ca(OH)_2$	6 M KOH + 1 M LiOH	100	0.89	–	0	25; 10	42.5	310	96.6	141	43.7	[C]
Stock et al., 2018[17]	Carbon mesh/ZnO/ionomeric hydroxide-conducting polymer (IHCP) core/shell structure 38.4% C mesh, 28.5% ZnO, 33.1% Fumasep FAA3	4 M KOH, saturated with ZnO	5.7	0.47	16	0.938	4.4; 4.4	40.5	124.5	75.0	67	8.34	[D]

Zhang et al., 2020[18]	ZnO nanorods coated with 30 nm TiO_2, on carbon paper substrate	4 M KOH + 2 M KF + 2 M K_2CO_3, saturated with ZnO	0.99	0.152	7.8	1.16	4.9; 0.99	92.7	92.6	92.7	33	3.06	[E]
Zhang et al., 2020[18]	ZnO nanorods coated with 30 nm TiO_2, on carbon paper substrate	4 M KOH + 2 M KF + 2 M K_2CO_3, saturated with ZnO	0.99	0.152	7.8	1.16	4.9; 0.99	39.8	39.7	–	180	7.15	[E]
Yan et al., 2018[14]	ZnO nanoparticles in "lasagna-like" GO matrix 71.4% ZnO nanoparticles, 8.9% GO, 8.9% carbon black, 10.7% water-based binder	4 M KOH + 2 M KF + 2 M K_2CO_3	0.66	0.714	6.05	0	3.0; 0.6	82.2	242	82.2	150	36.3	[F]

Notes:

All compositional percentages are weight percentages.

[A] $\bar{X}_{AM}$ accounts for the pre-dissolved ZnO in the electrolyte, but $\bar{q}_{dis}$ does not.

[B] Values are taken from the review by Stock et al.[12] except for Q_{AM}/A_{anode} (self-calculated).

[C] Values are taken from the review by Stock et al.,[12] but the performance metrics seem too high compared to the original paper by Parker et al.[16] The latter only says that the cell lasted 65 cycles at 40% Zn utilization and 141 cycles at >20% Zn utilization, not that the average Zn utilization was 42.5% over 141 cycles. In addition, the coulombic efficiency is reported in the review but is not found in the original paper. The amount of electrolyte is not reported in either source.

[D] Values are taken from the review by Stock et al.[12] except for Q_{AM}/A_{anode} (self-calculated). $\bar{X}_{AM}$ and $\bar{q}_{dis}$ do not account for pre-dissolved ZnO in electrolyte. Using the reported Q_E/Q_{AM} of 0.938, the $\bar{X}_{AM}$ and $\bar{q}_{dis}$ accounting for all active mass in the system are only 52% of the reported values.

[E] m_{AM}/m_{anode} does not account for the TiO_2 coating (whose mass was not reported). $\bar{X}_{AM}$ and $\bar{q}_{dis}$ do not account for pre-dissolved ZnO in electrolyte. Q_E/Q_{AM} is based on the zincate saturation concentration of 0.168 mol L^{-1} in the electrolyte previously reported by the same authors.[19] Using this value, the $\bar{X}_{AM}$ and $\bar{q}_{dis}$ accounting for all active mass in the system are only 46% of the reported values. The coulombic efficiency of the cell cycled at lower active material utilization was not reported.

[F] Values are taken from the review by Stock et al.[12] except for Q_{AM}/A_{anode} (self-calculated) and m_{AM}/m_{anode} (which appeared to be misreported).

4. References

1. Mauritz, K. A.; Moore, R. B., State of Understanding of Nafion. *Chemical Reviews* **2004,** *104* (10), 4535-4586.
2. Gebel, G., Colloidal Structure of Ionomer Solutions. In *Handbook of Fuel Cells - Fundamentals, Technology and Applications*, Vielstich, W.; Gasteiger, H.; Lamm, A.; Yokokawa, H., Eds. John Wiley & Sons, Ltd.: 2010.
3. Paul, D. K.; Karan, K.; Docoslis, A.; Giorgi, J. B.; Pearce, J., Characteristics of Self-Assembled Ultrathin Nafion Films. *Macromolecules* **2013,** *46* (9), 3461-3475.
4. Wang, Z.; Tang, H.; Li, J.; Zeng, Y.; Chen, L.; Pan, M., Insight into the structural construction of a perfluorosulfonic acid membrane derived from a polymeric dispersion. *Journal of Power Sources* **2014,** *256*, 383-393.
5. Bass, M.; Berman, A.; Singh, A.; Konovalov, O.; Freger, V., Surface Structure of Nafion in Vapor and Liquid. *The Journal of Physical Chemistry B* **2010,** *114* (11), 3784-3790.
6. Goswami, S.; Klaus, S.; Benziger, J., Wetting and Absorption of Water Drops on Nafion Films. *Langmuir* **2008,** *24* (16), 8627-8633.
7. Kelarakis, A.; Krysmann, M. J., Trivial and Non-Trivial Supramolecular Assemblies Based on Nafion. *Colloids and Interface Science Communications* **2014,** *1*, 31-34.
8. van Oss, C. J., *Interfacial Forces in Aqueous Media*. CRC Press, Taylor and Francis Group: New York, 2006.
9. Cannarella, J.; Liu, X.; Leng, C. Z.; Sinko, P. D.; Gor, G. Y.; Arnold, C. B., Mechanical Properties of a Battery Separator under Compression and Tension. *Journal of The Electrochemical Society* **2014,** *161* (11), F3117-F3122.
10. Kim, Y.-H.; Oblas, D.; Angelopoulos, A. P.; Fossey, S. A.; Matienzo, L. J., Adsorption of a Cationic Polyacrylamide onto the Surface of a Nafion Ionomer Membrane. *Macromolecules* **2001,** *34* (21), 7489-7495.
11. Duay, J.; Lambert, T. N.; Aidun, R., Stripping Voltammetry for the Real Time Determination of Zinc Membrane Diffusion Coefficients in High pH: Towards Rapid Screening of Alkaline Battery Separators. *Electroanalysis* **2017,** *29* (10), 2261-2267.
12. Stock, D.; Dongmo, S.; Janek, J.; Schröder, D., Benchmarking Anode Concepts: The Future of Electrically Rechargeable Zinc–Air Batteries. *ACS Energy Letters* **2019,** *4* (6), 1287-1300.
13. Turney, D. E.; Gallaway, J. W.; Yadav, G. G.; Ramirez, R.; Nyce, M.; Banerjee, S.; Chen-Wiegart, Y.-c. K.; Wang, J.; D'Ambrose, M. J.; Kolhekar, S.; Huang, J.; Wei, X., Rechargeable Zinc Alkaline Anodes for Long-Cycle Energy Storage. *Chemistry of Materials* **2017,** *29* (11), 4819-4832.
14. Yan, Y.; Zhang, Y.; Wu, Y.; Wang, Z.; Mathur, A.; Yang, H.; Chen, P.; Nair, S.; Liu, N., A Lasagna-Inspired Nanoscale ZnO Anode Design for High-Energy Rechargeable Aqueous Batteries. *ACS Applied Energy Materials* **2018,** *1* (11), 6345-6351.
15. Lim, M. B.; Lambert, T. N.; Ruiz, E. I., Effect of ZnO-Saturated Electrolyte on Rechargeable Alkaline Zinc Batteries at Increased Depth-of-Discharge. *Journal of The Electrochemical Society* **2020,** *167* (6), 060508.
16. Parker, J. F.; Chervin, C. N.; Pala, I. R.; Machler, M.; Burz, M. F.; Long, J. W.; Rolison, D. R., Rechargeable nickel–3D zinc batteries: An energy-dense, safer alternative to lithium-ion. *Science* **2017,** *356* (6336), 415.
17. Stock, D.; Dongmo, S.; Damtew, D.; Stumpp, M.; Konovalova, A.; Henkensmeier, D.; Schlettwein, D.; Schröder, D., Design Strategy for Zinc Anodes with Enhanced Utilization and Retention: Electrodeposited Zinc Oxide on Carbon Mesh Protected by Ionomeric Layers. *ACS Applied Energy Materials* **2018,** *1* (10), 5579-5588.

18. Zhang, Y.; Wu, Y.; You, W.; Tian, M.; Huang, P.-W.; Zhang, Y.; Sun, Z.; Ma, Y.; Hao, T.; Liu, N., Deeply Rechargeable and Hydrogen-Evolution-Suppressing Zinc Anode in Alkaline Aqueous Electrolyte. *Nano Letters* **2020,** *20* (6), 4700-4707.
19. Zhang, Y.; Wu, Y.; Ding, H.; Yan, Y.; Zhou, Z.; Ding, Y.; Liu, N., Sealing ZnO nanorods for deeply rechargeable high-energy aqueous battery anodes. *Nano Energy* **2018,** *53*, 666-674.